Design of a High-Efficiency Broadband Asymmetric Doherty Power Amplifier

Bin Wang[*]**, Jiang Teng, Debao Zhang, and Dong Su**

Abstract—This study proposes a broadband asymmetric Doherty power amplifier (A-DPA) with a broadband matching network and an improved power combination network (PCN). A broadband matching network in the form of a low-pass filter is analyzed and applied in this work. With the narrowband characteristic of a 1/4 wavelength transmission line, an improved PCN is also analyzed and applied to decrease the impedance transformation ratio of the 1/4 wavelength transmission line and then extend the working bandwidth of the DPA. In the design process, GaN HEMTs from Cree are selected to be the main and auxiliary power amplifier transistors, and the ADS software is used to complete the entire design process. In the working frequency band of 3.3 GHz–3.6 GHz, simulated results show that the gain is approximately 13 dB when the output power is lower than 40 dBm and that the power-added efficiency (PAE) is 39%–51% within the 9 dB power back-off (PBO) region. Measured results indicate that the proposed A-DPA exhibits a 36%-45% PAE within the 9 dB PBO region. The saturated PAE is between 58% and 62%, and the saturated output power is approximately 42 dBm.

1. INTRODUCTION

Radio frequency power amplifiers (RFPAs) are one of the most important components of transmitters in wireless communication systems. The output power, gain, efficiency, and linearity of RFPAs have a vital impact on the performance of transmitters. The Doherty power amplifier [1] (DPA) can maintain a high efficiency within a certain power back-off (PBO) region, thereby overcoming the disadvantages of traditional class AB power amplifiers (PAs) to avoid non-linear distortion and work away from the saturation region; however, it results in low efficiency. Therefore, DPAs are widely used in current transmitters.

However, the PBO region of the conventional symmetric DPA is only approximately 6 dB [2–5] while the peak-to-average power ratio (PAPR) of the 4G LTE signal is 6 dB–12 dB. Thus, the symmetric DPA cannot meet the requirements of current transmitters. Various technologies, such as the power control technology [6], harmonic injection [7], and asymmetric structure [8–10], have been introduced to extend the PBO region of DPAs. Among these technologies, asymmetric structure is the most widely used because of its simple structure and design process. An asymmetric DPA (A-DPA) consists of an uneven power divider, main and auxiliary PA branches using different transistors, and a power combination network (PCN). In general, the main PA is biased on class-AB condition and the auxiliary PA is biased on class-C condition, the theory and validation of the AB-C DPA have been discussed in detail in [11, 12], and the bias conditions are also adopted in this work.

Although the DPA can maintain a good efficiency within a certain PBO region and achieve balance between efficiency and linearity, its working bandwidth is narrow. After the use of the carrier aggregation technology in a 4G LTE communication system, the maximum bandwidth can reach 100 MHz [13],

thereby posing corresponding challenges to the working bandwidth of the DPA. According to the structural analysis of DPAs, one of the main reasons for the narrow bandwidth is the 1/4 wavelength transmission line in the PCN [14]. The 1/4 wavelength transmission line is necessary for impedance transformation and power combination during the DPA operation, and its working bandwidth will decrease as its impedance transformation ratio (ITR) increases. Therefore, numerous works are currently focused on the PCN to extend the working bandwidth of DPAs, for example, post-matching [15–17] and power compensation network [18]; these technologies have also improved the working bandwidth of DPAs significantly.

A broadband matching network is indispensable to a broadband DPA. Three main broadband design methods exist. The first method is the simplified real frequency technology [19, 20], which employs the synthetic transfer function to derive the entire matching network topology. The second method is based on small reflection theory [21], which aims to use transmission lines with different characteristic impedances to construct an impedance converter. The third method is based on the low-pass filter prototype [22]. Among the three methods above, the first method is the most universal, but its design process is the most complex, and it lacks effective control of harmonic impedance. Sometimes, the size of the broadband matching network may be extremely large when using the second method. Meanwhile, the third method is selected for the design of the broadband matching network in this work because of its simple design process and excellent broadband matching characteristics.

In this work, a broadband A-DPA with an improved matching network and a PCN is proposed. The working frequency band is 3.3 GHz–3.6 GHz, which is one of the main working bands for future 5G. In Section 2, the bandwidth limitation of the conventional DPA configuration is discussed in view of the 1/4 wavelength transmission line in the PCN; we adopt an improved PCN [8] to extend the bandwidth of the DPA by decreasing the ITR. We also present the analysis and design process of the broadband matching network in low-pass filter form. In Sections 3 and 4, the implementation processes of the simulation and measurement of the A-DPA are explained in detail, and all results are presented. With the broadband matching network and the improved PCN, the proposed A-DPA exhibits a relatively excellent performance and can be applied to mobile communication stations.

2. ANALYSIS OF POWER COMBINATION AND BROADBAND MATCHING NETWORKS

2.1. Power Combination Network

DPAs have two major working states, namely, the low and saturation power states. When a DPA works in low power state, only the main PA is on operating. The main PA is forced to be saturated first because its load impedance is matched to a high impedance and the DPA obtains its peak efficiency for the first time. With an increase in input power, the auxiliary PA starts to operate. Under the action of active load modulation, the load impedance of the main PA gradually decreases with that of the auxiliary PA decreases. When the auxiliary PA reaches saturation, the DPA obtains its peak efficiency for the second time. Therefore, the PCN is required to simultaneously allow the active load modulation and the output matching [23], and adjust and combine the load impedance of the main and auxiliary PAs during the DPA operation.

The PCN consists of two 1/4 wavelength transmission lines, namely, the impedance adjustment line (IDL) at the output of the main PA and the impedance combination line (ICL) before the DPA output. The IDL is mainly used to transform the load impedance of the main PA between the low and saturation power states. The ICL is mainly used to convert the parallel impedance of the main PA and auxiliary PA into the load impedance of the DPA. Consequently, the 1/4 wavelength transmission line plays a vital role in the DPA configuration. The bandwidth characteristics of the 1/4 wavelength transmission line can be expressed as follows:

$$BMW = \frac{\Delta f}{f_0} = 2 - \frac{4}{\pi} \arccos \left[\frac{\Gamma_m}{\sqrt{1 - \Gamma_m^2}} \frac{2\sqrt{Z_{in}Z_L}}{|Z_L - Z_{in}|} \right] \tag{1}$$

$$r = \frac{Z_{in}}{Z_L} \tag{2}$$

where Γ_m is the reflection coefficient; Z_{in} and Z_L are the input and output impedances of the transmission line, respectively; and r is the ITR. Obviously, Eq. (1) indicates that when the reflection coefficient (Γ_m) is a certain value, the working bandwidth of the transmission line can be effectively extended by decreasing the ITR for the benefit of the working bandwidth of the DPA.

Generally, conventional DPAs with two branches only obtain a PBO region of 6 dB mainly because they are composed of main and auxiliary PAs of the same size. In extending the PBO region of DPAs, the saturated output power of the main PA should be less than that of the auxiliary PA. The power divider should also be designed as an unequal power divider to drive additional input power to the auxiliary PA to compensate for its low power gain when it operates in the class-C mode. The PBO region can be expressed as

$$PBO = 20\log(1+\delta) \tag{3}$$

$$\delta = \frac{P_{A,Sat}}{P_{M,Sat}} \tag{4}$$

where $P_{M,Sat}$ and $P_{A,Sat}$ are the saturated output powers of the main and auxiliary PAs, respectively. In this work, the main and auxiliary PAs are selected from Cree's GaN HEMTs CGH40006P and CGH40010F, and the typical output powers for the two transistors are 6 and 10 W, respectively. δ is approximately equal to 2. Therefore, a 9.5 dB PBO region can be achieved theoretically. However, by adjusting the gate bias voltage and power division ratio of the power divider, a large PBO can be obtained in actual applications.

In the conventional asymmetric DPA configuration, the load impedances of the main and auxiliary PAs under the low and saturation power states are respectively expressed as

$$Z_{M1} = \begin{cases} (1+\delta)\,Z_0 & @\text{Low} \\ Z_0 & @\text{Sat} \end{cases} \tag{5}$$

$$Z_{A1} = \begin{cases} \infty & @\text{Low} \\ \dfrac{Z_0}{\delta} & @\text{Sat} \end{cases} \tag{6}$$

where Z_0 is the load impedance of the DPA, which is equal to 50 Ω. The characteristic impedances of the IDL and ICL are respectively expressed as

$$Z_1 = Z_0 \tag{7}$$

$$Z_2 = \frac{Z_0}{\sqrt{1+\delta}} \tag{8}$$

For the improved PCN adopted in this work, the corresponding load impedances of the main and auxiliary PAs under the low and saturation power states are respectively expressed as

$$Z'_{M1} = \begin{cases} (1+\delta) & @\text{Low} \\ Z_0 & @\text{Sat} \end{cases} \tag{9}$$

$$Z'_{A1} = \begin{cases} \infty & @\text{Low} \\ Z_0 & @\text{Sat} \end{cases} \tag{10}$$

and the characteristic impedances of the IDL and ICL for the improved PCN are respectively expressed as

$$Z'_1 = \sqrt{\delta}\,Z_0 \tag{11}$$

$$Z'_2 = \sqrt{\frac{\delta}{1+\delta}} \cdot Z_0 \tag{12}$$

Finally, the conventional and improved PCNs can be calculated (Fig. 1).

Figure 1 indicates that employing the improved PCN can enlarge the PBO region and extend its working bandwidth. In addition, the output impedance of the auxiliary PA in the conventional PCN is 25 Ω, but most RF devices in current RF communication systems have an interface impedance of 50 Ω. Thus, an additional matching network must be designed to transform the output impedance from 50 to 25 Ω in the conventional PCN, which is more complex than the improved PCN.

(a) Conventional   (b) Improved
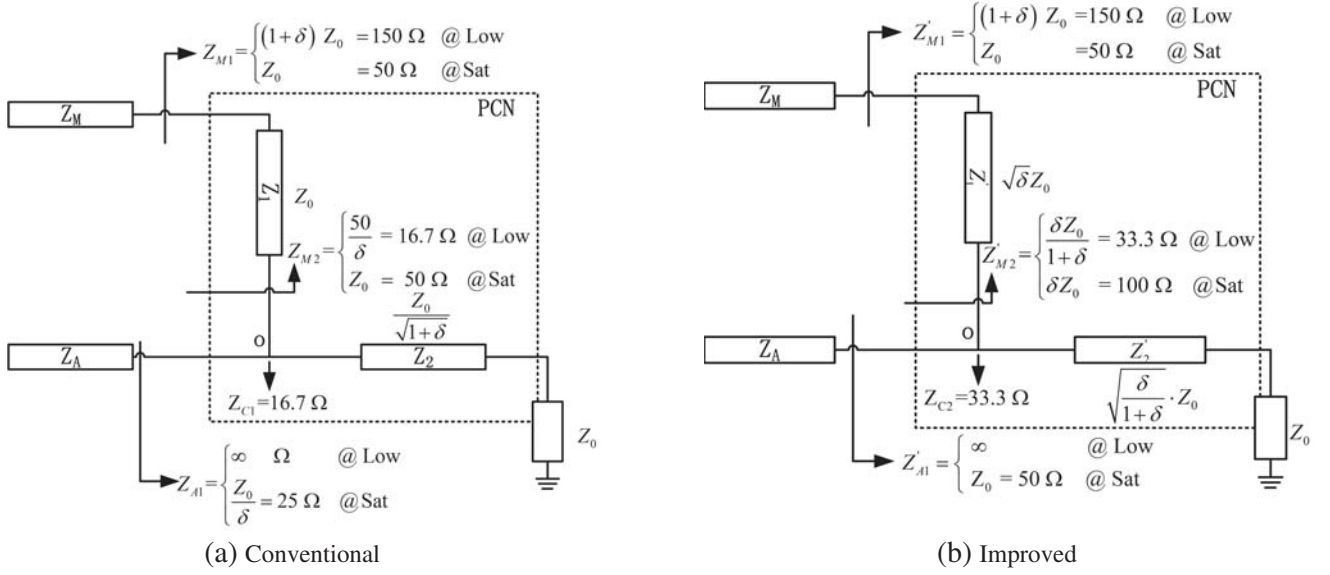
Figure 1. PCNs: (a) conventional and (b) improved.

2.2. Broadband Matching Network

The matching network is an important part of the PA. Its performance has a direct impact on the performance of the PA. If the input matching network (IMN) is not well designed, a strong reflection will occur and cause the deterioration of the output power and efficiency while potentially damaging the pre-amplifier or test instrument. The output matching network (OMN) usually affects the gain and then affects the output power and efficiency of the PA. Therefore, a broadband matching network is indispensable to a broadband PA. In this work, broadband matching networks in low-pass filter form [22] are selected to be the IMN and OMN. The broadband matching network is designed in three main steps.

Step 1) Design of prototype matching network

The source and load impedance must be found before designing the IMN and OMN. Generally, the data sheet of transistors provides a reference impedance in some frequency points. After using the active load-pull system in the ADS software, a reasonably accurate impedance can be obtained. In this work, Fig. 2 shows the result of the active load-pull method for the auxiliary PA transistor CGH400010F taken as an example. In Fig. 2, the thin blue lines represent the output power contours, and the thick red line represent the power-added efficiency (PAE) contours. Under this condition, the maximum output power and the PAE are 43.1 dBm and 66.7%, respectively, and the corresponding load impedance is $18 - j \cdot 1\,\Omega$ at the center frequency of 3.45 GHz. The ITR of the OMN is $r = 50/18 \approx 3$, the in-band ripple is $L_{AR} < 0.1\,\text{dB}$, the relative bandwidth is 20%, and order n is 4, as shown in the tables in [24]. Finally, the corresponding prototype matching network is shown in Fig. 3.

Step 2) Design of lumped element matching networks

The prototype matching network is transformed to a $50\,\Omega$ system at the center frequency of 3.45 GHz with lumped elements using the following transformation formulas:

$$L_n = g_{2n-1} \cdot \frac{\omega_0}{\omega_1} \cdot \frac{50}{r} \tag{13}$$

$$C_n = g_{2n} \cdot \frac{\omega_0}{\omega_1} \cdot \frac{r}{50} \tag{14}$$

where ω_1 is the angular frequency at the frequency of 3.45 GHz, and ω_0 is the normalized angular frequency, which is 1 rad/s. The transformation process is usually divided into two steps. First, the input and output impedances are set to $18\,\Omega$ and $50\,\Omega$, respectively, to complete the matching of real-to-real impedance (LumR-R). Second, the input impedance is set to $18 + j \cdot 1\,\Omega$ (conjugate to the impedance
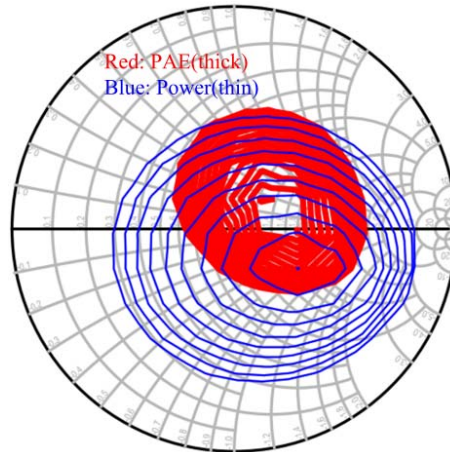
Figure 2. Results of active load-pul.
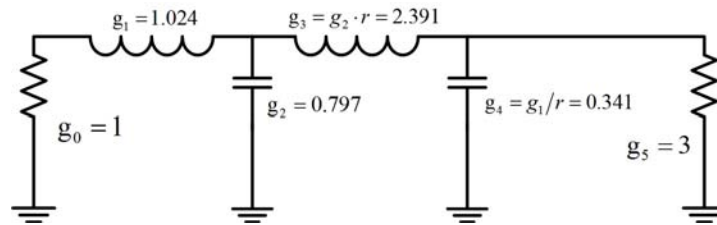
Figure 3. Prototype of matching network.
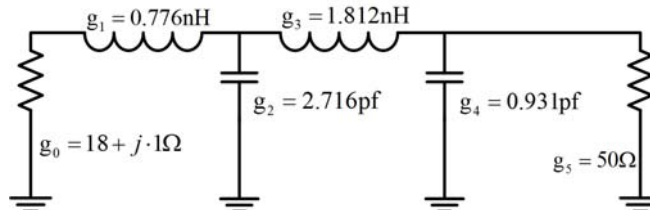
Figure 4. Matching network with lumped elements.

obtained in the load-pull) to complete the matching of real-to-imaginary impedance (LumR-I). In this design process, the values of capacitors and inductors are properly turned by using the ADS software to obtain the optimal result. The matching network with lumped elements is shown in Fig. 4.

Step 3) Design of distributed element matching network

Owing to the parasitic parameter effect on lumped elements in high frequency and the inconvenience for later physical debugging, lumped elements are usually replaced by distributed elements. According to the Kuroda rule and Richard change [21], the inductor can be replaced by a high-impedance transmission line, and the capacitor can be replaced by a low-impedance open-circuit stub. Hence, the lengths of the high-impedance line and open-circuit stub are respectively calculated as

$$l_L = \frac{v_p L}{Z_L} \tag{15}$$

$$l_C = \frac{\arctan(2\omega_1 Z_c C)}{\beta} \tag{16}$$

where Z_L is the characteristic impedance of the line and Z_C is the characteristic impedance of the stub. ν_p and β are the phase velocity and propagation constant, respectively; they can be correspondingly

calculated as

$$v_p = \frac{v_0}{\sqrt{\varepsilon_{re}}} \tag{17}$$

$$\beta = \frac{2\pi}{\lambda} \tag{18}$$

$$\varepsilon_{re} = \frac{\varepsilon_r + 1}{2} + \frac{\varepsilon_r - 1}{2} \frac{1}{\sqrt{1 + 12h/w}} \tag{19}$$

where ε_r and h are the relative dielectric constant of 3.48 and the thickness of the dielectric substrate of 0.508 mm for the Ro4350B dielectric substrate selected in this work. ε_{re} is the effective dielectric constant.

Notably, owing to the differences in the transmission characteristics between the lumped and distributed elements, it must be debugged and optimized repeatedly through the ADS software to achieve the desired results.

Finally, the matching network with distributed elements is shown in Fig. 5, and the simulated results of the above networks are shown in Fig. 6. The results in Fig. 6 indicate that the matching network used in this work has an advantage in broadband matching. The result of the matching network with distributed elements (DisR-I) shows that S_{11} in the working frequency band is lower than -24 dB, which fully satisfies the requirements in this work.
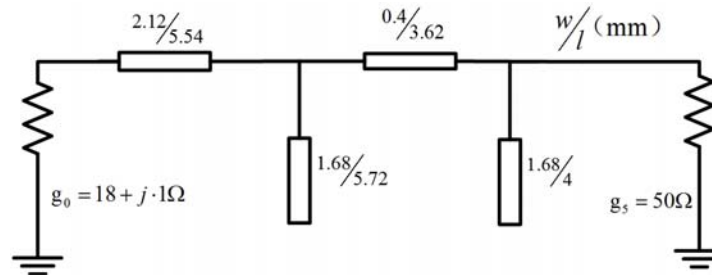
Figure 5. Matching network with distributed elements.
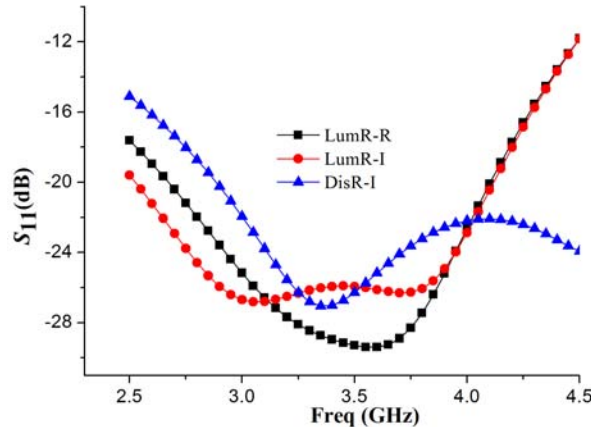
Figure 6. Simulated results of S_{11}.

3. DESIGN AND SIMULATION

Currently, third-generation semiconductors represented by SiC and GaN are widely used in current PAs because of their numerous advantages, such as broadband working bandwidth, wide bandgap, and high

electron mobility. Therefore, GaN HEMTs from Cree are chosen for simulation and implementation in this work. CGH40006P is chosen as the main PA transistor, and CGH40010F is chosen as the auxiliary PA transistor. The main PA is biased at $V_{gs} = -2.93\,\text{V}$ and $V_{ds} = 28\,\text{V}$ under class AB mode. The quiescent current I_{DQ} is 100 mA. The auxiliary PA is biased at $V_{gs} = -6\,\text{V}$ and $V_{ds} = 28\,\text{V}$ under class C mode. All simulations are conducted using the ADS software from Agilent.

A power divider is used to divide the input signal into the main and auxiliary PAs. If the power division ratio is extremely large, excessive input signal will be driven to the main PA. Consequently, the PBO point may be withdrawn earlier, and the gain of the main PA will be compressed seriously while the auxiliary PA starts to operate. On the contrary, if the power division ratio is extremely small, excessive input signals will be driven to the auxiliary PA, which will cause a strong nonlinear distortion because it operates in class C mode. Therefore, the ideal working state for the power divider is to drive additional input signal to the main PA before the auxiliary PA starts to operate and then drive additional input signal to the auxiliary PA after the auxiliary PA starts to operate. However, once the microstrip line power divider is finished, adjusting it becomes difficult. In this work, through repeated debugging and the comparisons of the simulated results, the power division ratio is set to 1 : 1.5, and a Wilkinson power divider is adopted.

The simulated results of the power divider are shown in Fig. 7. In the working frequency band, S_{23} is lower than $-28\,\text{dB}$, indicating the good isolation between the output ports; S_{11}, S_{22}, and S_{33} are all lower than $-25\,\text{dB}$; and S_{21} and S_{31} are 4.1 dB and 2.3 dB, respectively, at the center frequency of 3.45 GHz.
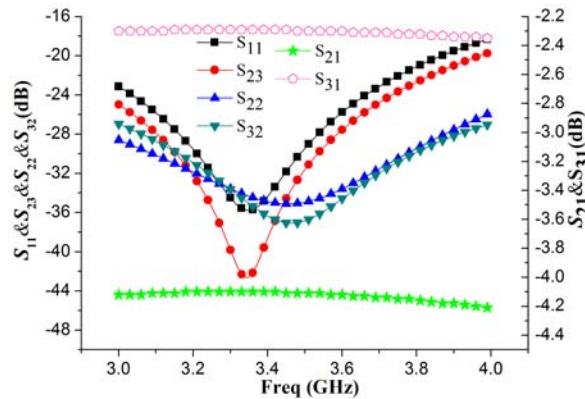
Figure 7. Simulated results of power divider.

As for the main and auxiliary PAs, their design processes are nearly the same, including the matching network and bias circuit designs. The matching network is chosen from the matching topology network elaborated in Section 2. Using the same matching topology network can reduce the phase difference between the main and auxiliary PA branches and thereby benefit the combination of output power and achieve a high PAE. A 1/4 wavelength transmission is chosen as the bias circuit. In general, the transmission line is required to be as narrow as possible when it serves as the bias circuit. However, if the transmission line is extremely thin, it may burn when a high current passes through. In this work, the width of the transmission lines for the gate and drain circuits are 0.3 and 0.8 mm, respectively. Moreover, a $10\,\Omega$ resistance is connected in series to the bias circuit to prevent the DPA from producing low frequency self-excitation. A series of capacitors with pF, nF, and μF values are added to the bias circuit to prevent the mutual interference between the RF signal and the DC power supply. Considering that PAs are highly sensitive to source impedance, the position of the bias circuits is moved forward before the IMNs in the design of the main and auxiliary PAs.

Finally, by combining the power divider, main PA, auxiliary PA, and PCN, the entire A-DPA is obtained. In addition, input and output offset lines are added before the IMN and after the OMN to accelerate the debugging. The configuration of the proposed A-DPA is shown in Fig. 8.

As shown in Fig. 9(a), the gain is approximately 13 dB when the output power is lower than 40 dBm, and the saturated output power is over 43 dBm in the working frequency band. Fig. 9(b) indicates that
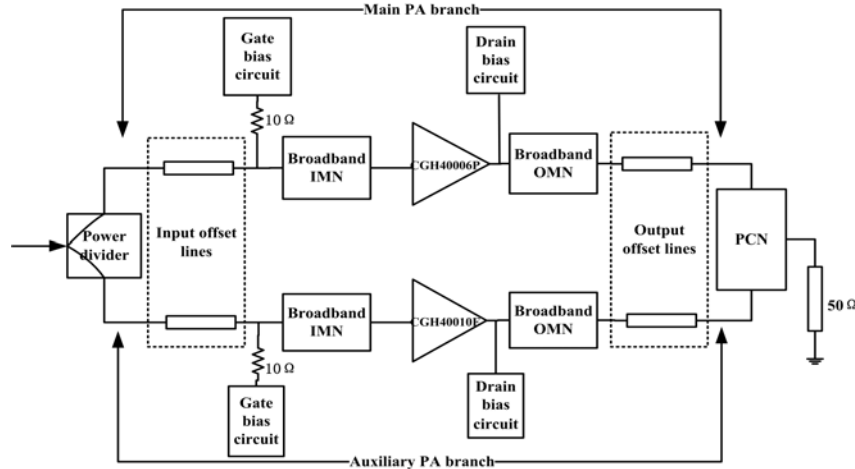
Figure 8. A-DPA configuration.

(a) Gain	(b) PAE
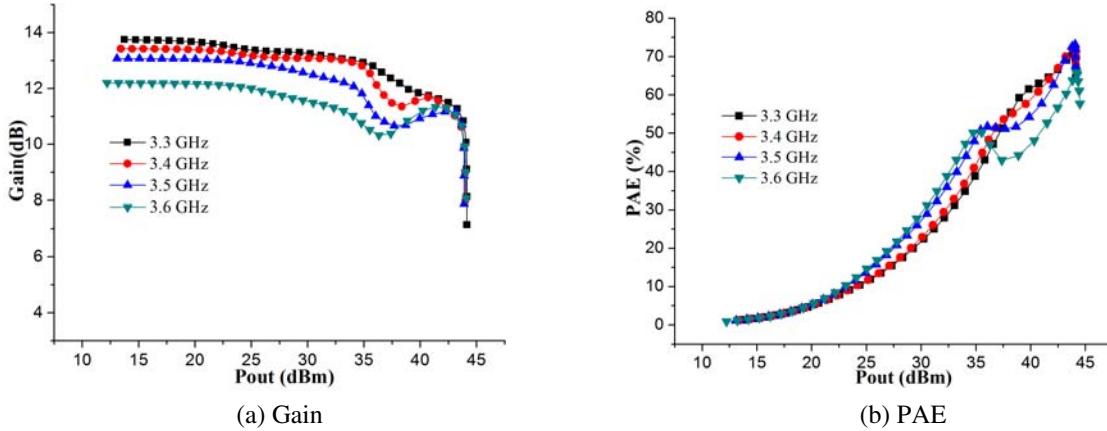
Figure 9. Simulated results of (a) gain and (b) PAE.

the saturated PAE ranges from 66%–70% and that the PAE is 39%–51% within the 9 dB PBO region. In the deep PBO region (10 dB OBO), the PAE is maintained above 45% at 3.5 GHz and 3.6 GHz.

4. IMPLEMENTATION AND MEASUREMENT RESULTS

To further validate the performances of the proposed A-DPA, we fabricate it on a Ro4350B substrate with copper metallization (Ro4350B with relative dielectric constant $\varepsilon_r = 3.48$, substrate height $H = 0.508$ mm, metal thickness $t = 0.035$ mm). A 6 mm-thick aluminum plate is placed under the substrate to achieve effective heat dissipation. The photograph of the fabricated A-DPA is shown in Fig. 10; the size of the entire A-DPA is 12.6 cm×7.2 cm.

During measurement, strict attention must be paid to the power-on and power-off sequences. The power-on sequence should be for the gate voltage first and then for the drain voltage next; the opposite is true for the power-off sequence. Due to the fact that the differences between the large signal simulation model and an actual PA transistor, the gate voltage is determined according to the quiescent current. The gate voltage of the main and auxiliary PAs are −2.57 and −6 V, respectively; the drain voltages are all 28 V; and the quiescent is 100 mA. Owing to the matching errors and the environmental differences between the simulation and the measurement, numerous works will be conducted to debug and optimize the proposed A-DPA.

The measured results of the gain and PAE are shown in Fig. 11. First, signal tone continuous

wave measurements are performed in the working frequency band of 3.3 GHz–3.6 GHz. As shown in Fig. 11(a), the gain is approximately 13 dB, and the saturated output power is approximately 42 dBm. From Fig. 11(b), the proposed A-DPA achieves a PAE of 36%–45% within the 9 dB PBO region, and the saturated PAE is 58%–62%. Second, to measure the linearity of the proposed A-DPA, we apply a 32 QAM modulated signal with 10 MHz of bandwidth generated by the Agilent signal generator E4438C in the measurement of the ACPR at the frequency of 3.4 GHz. The ACPR is measured with a channel integration bandwidth of 10 MHz at ±12.5 MHz offset from 3.4 GHz. Fig. 12 shows that the result of the ACPR is −25.6 dBc at the output power of 29 dBm. Table 1 provides the performance of the recently proposed broadband DPAs. The comparison of performance in Table 1 indicates that when the working bandwidth extends, the efficiency decreases, indicating that a high efficiency broadband DPA with a large PBO region should remain a priority in PA research.
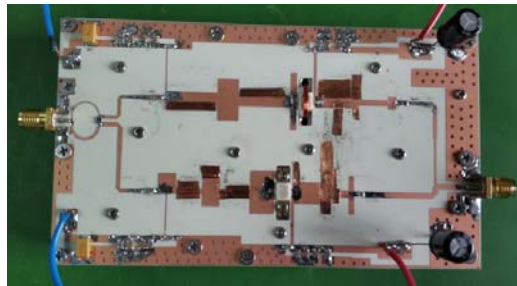
Figure 10. Photograph of proposed A-DPA.

| (a) Gain | (b) PAE |
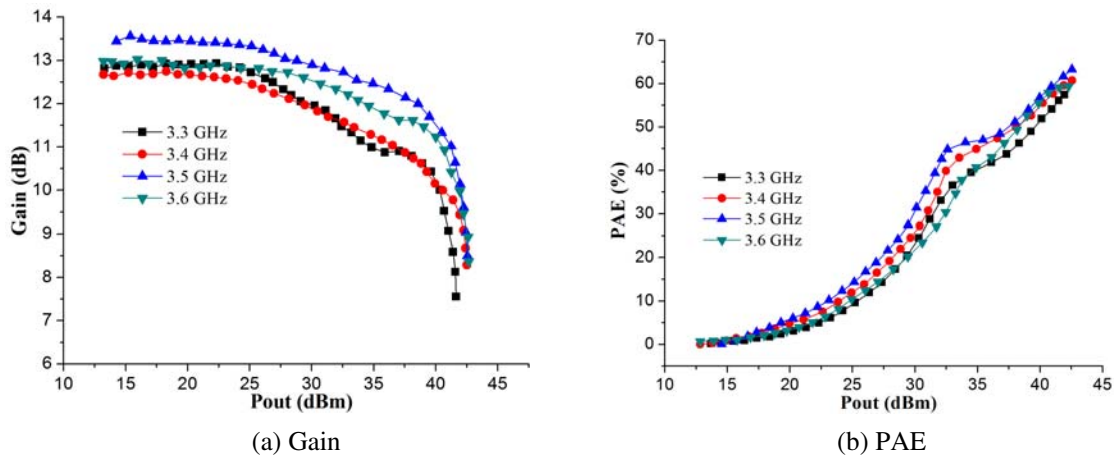
Figure 11. Measured results of (a) gain and (b) PAE.

Table 1. Performances of recently proposed broadband DPAs.

Ref	Year	Freq(GHz)	BW(MHz)	Eff_Sat(%)	Eff_PBO(%)
[25]	2014	1.05–2.55	1500	45–83@DE*	35–58@6 dB&DE
[26]	2015	1.63–1.98	350	44–60@PAE	20–49@6 dB&PAE
[27]	2016	2.0-2.6	600	53–76@DE	≥ 40@8 dB&DE
[28]	2018	3.3–3.75	450	58–71@DE	44–55@8 dB&DE
[29]	2018	1.5–2.6	1100	40–55@DE	31–35@6 dB&DE
T.W	2019	3.3–3.6	300	58–62@PAE	36–45@9 dB&PAE

*DE is drain efficiency
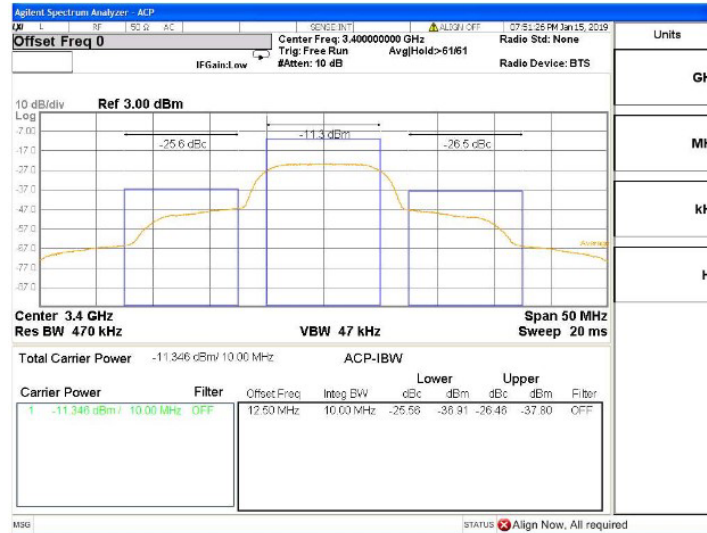
Figure 12. Measured result of ACPR.

5. CONCLUSION

A broadband A-DPA with an improved PCN and broadband matching network is presented in this paper. By using the improved PCN and broadband matching network, the working bandwidth of the proposed A-DPA can be effectively extended. Moreover, enhanced efficiency and PBO origin can be achieved simultaneously using an unequal power divider with a power division of 1:1.5 and different PA transistors for the main and auxiliary PAs. Finally, in the working frequency band, the measured results show that the proposed A-DPA achieves a PAE of 36%–45% within the 9 dB PBO origin and that the saturated output power is approximately 42 dBm. All the measured results indicate that the proposed design strategy offers some advantages in improving the working bandwidth, efficiency, and PBO region of DPAs.

ACKNOWLEDGMENT

REFERENCES

1. Doherty, W. H., "A new high efficiency power amplifier for modulated waves," *Proceedings of the Institute of radio engineers*, Vol. 24, No. 9, 1163–1182, 1936.
2. Ahn, G. H., M. S. Kim, H. C. Park, and Y. G. Yang, "Design of a high efficiency and high-power inverted Doherty amplifier," *IEEE Transactions on Microwave Theory and Techniques*, Vol. 55, No. 6, 1105–1111, 2007.
3. Lee, Y. S., M. W. Lee, and Y. H. Jeong, "Highly linear power tracking Doherty amplifier for WCDMA repeater applications," *IEEE Microwave and Wireless Components Letters*, Vol. 18, No. 7, 485–487, 2008.
4. Liu, Q.-A., S.-B. He, and W.-M. Shi, "Design of 3.5 GHz linear high efficiency Doherty power amplifier with pre-matching," *2015 Asia Pacific Microwave Conference (APMC)*, 1–3, Nan Jing, 2015.
5. Xia, J., M. Yang, Y. Guo, and A. Zhu, "A broadband high-efficiency Doherty power amplifier with integrated compensating reactance," *IEEE Transactions on Microwave Theory and Techniques*, Vol. 64, No. 7, 2014–2024, 2016.

6. Qi, T. and S. He, "Design of high efficiency Doherty power amplifier applying power controlling technology with 15 dB output power back-off," *2017 47th European Microwave Conference (EuMC)*, 576–579, Nuremberg, 2017.

7. Zhou, X., S. Zheng, W. Chan, X. Fang, and D. Ho, "Post matching Doherty power amplifier with extended back-off range based on self-generated harmonic injection," *IEEE Transactions on Microwave Theory and Techniques*, Vol. 66, No. 4, 1951–1963, 2018.

8. Son, J., I. Kim, J. Moon, J. Lee, and B. Kim, "A highly efficient asymmetric Doherty power amplifier with a new output combining circuit," *2011 IEEE International Conference on Microwaves, Communications, Antennas and Electronic Systems (COMCAS 2011)*, 1–4, TelAviv, 2011.

9. Jang, D., J. Choi, and J. Kim, "Asymmetric Doherty power amplifier with optimized characteristics in output power back-off range between 6 dB and 10 dB," *The 40th European Microwave Conference*, 870–873, Paris, 2010.

10. Iwamoto, M., A. Williams, P.-F. Chen, A. G. Metzger, L. E. Larson, and P. M. Asbeck, "An extended Doherty amplifier with high efficiency over a wide power range," *IEEE Transactions on Microwave Theory and Techniques*, Vol. 49, No. 12, 2472–2479, 2001.

11. Colantonio, P., F. Giannini, R. Giofrè, and L. Piazzon, "The AB-C Doherty power amplifier. Part I: Theory," *International Journal of RF and Microwave Computer-Aided Engineering*, Vol. 19, No. 3, 293–306, 2009.

12. Colantonio, P., F. Giannini, R. Giofrè, and L. Piazzon, "The AB-C Doherty power amplifier. Part II: validation," *International Journal of RF and Microwave Computer-Aided Engineering*, Vol. 19, No. 3, 307–316, 2009.

13. Parkvall. S., A. Furuskär, and E. Dahlman, "Evolution of LTE toward IMT-advanced," *IEEE Transactions on Communication Magazine*, Vol. 49, No. 2, 84–91, 2011.

14. Sun, G. and R. H. Jansen, "Broadband Doherty power amplifier via real frequency technique," *IEEE Transactions on Microwave Theory and Techniques*, Vol. 60, No. 1, 99–111, 2012.

15. Kwon, J., M. Seo, H. Lee, J. Gu, J. Ham, K. C. Hwang, and K. Lee, "Broadband Doherty power amplifier based on asymmetric load matching networks," *IEEE Transactions on Circuits and Systems II: Express Briefs*, Vol. 62, No. 6, 533–537, 2015.

16. Pang, J., S. He, Z. Dai, C. Huang, J. Peng, and F. You, "Design of a post-matching asymmetric Doherty power amplifier for broadband applications," *IEEE Microwave and Wireless Components Letters*, Vol. 26, No. 1, 52–54, 2016.

17. Pang, J., S. He, C. Huang, Z. Dai, J. Peng, and F. You, "A post-matching Doherty power amplifier employing low-order impedance inverters for broadband applications," *IEEE Transactions on Microwave Theory and Techniques*, Vol. 63, No. 12, 4061–4071, 2015.

18. Rubio, J. M., J. Fang, V. Camarchia, R. Quaglia, M. Pirola, and G. Ghione, "3–3.6 GHz wideband GaN Doherty power amplifier exploiting output compensation stages," *IEEE Transactions on Microwave Theory and Techniques*, Vol. 60, No. 8, 2543–2548, 2012.

19. Sun, Y. and X. Zhu, "Broadband continuous class-F^{-1} amplifier with modified harmonic-controlled network for advanced long term evolution application," *IEEE Microwave and Wireless Components Letters*, Vol. 25, No. 4, 250–252, 2015.

20. Aridas, N. K., B. S. Yarman, and P. Chacko, "Wideband power amplifier for two-way radio applications via real-frequency technique," *Electronics Letters*, Vol. 50, No. 23, 1762–1764, 2014.

21. Pozar, D. M., *Microwave Engineering*, 3rd Edition, Publishing House of Electronics Industry, 2015.

22. Chen, K and D. Peroulis, "Design of highly efficient broadband class-E power amplifier using synthesized low-pass matching networks," *IEEE Transactions on Microwave Theory and Techniques*, Vol. 59, No. 12, 3162–3173, 2011.

23. Giofrè, R., P. Colantonio, F. Giannini, and L. Piazzon, "New output combiner for Doherty amplifiers," *IEEE Microwave and Wireless Components Letters*, Vol. 23, No. 1, 31–33, 2013.

24. Matthaei, G. L., "Tables of Chebyshev impedance transformation networks of low-pass filter form," *Proceedings of the IEEE*, Vol. 52, No. 8, 939–963, 1964.

25. Giofrè, R., L. Piazzon, P. Colantonio, and F. Giannini, "An ultra-broadband GaN Doherty amplifier with 83% of fractional bandwidth," *IEEE Microwave and Wireless Components Letters*, Vol. 24, No. 11, 775–777, 2014.

26. Watanabe, S., Y. Takayama, R. Ishikawa, and K. Honjo, "A miniature broadband Doherty power amplifier with a series-connected load," *IEEE Transactions on Microwave Theory and Techniques*, Vol. 63, No. 2, 572–579, 2015.

27. Chen, C., P. Qiao, G. Wang, Z. Cheng, and Q. Xue, "A broadband three-device Doherty power amplifier based on a modified load modulation network," *2016 IEEE MTT-S International Microwave Symposium (IMS)*, 1–4, San Francisco, CA, 2016.

28. Huang, C., S. He, and F. You, "Design of broadband modified class-J Doherty power amplifier with specific second harmonic terminations," *IEEE Access*, Vol. 6, 2531–2540, 2018.

29. Khan, M. S., H. Zhang, X. Wang, R. Ullah, I. Ahmad, S. Shahzad, Q. A. Arain, and M. Z. Tunio, "A novel two-stage broadband Doherty power amplifier for wireless applications," *IEEE Microwave and Wireless Components Letters*, Vol. 28, No. 1, 40–42, 2018.